Available online at www.sciencedirect.com
ScienceDirect
Computers and Structures 84 (2006) 2244–2253
Computers & Structures
www.elsevier.com/locate/compstruc

The simulation of 3D elastic scattering produced by thin rigid inclusions using the traction boundary element method

António Tadeu *, Paulo Amado Mendes, Julieta António

Department of Civil Engineering, University of Coimbra, Pólo II – Pinhal de Marrocos, 3030-290 Coimbra, Portugal

Received 17 April 2006; accepted 7 August 2006
Available online 25 October 2006

Abstract

A mixed formulation that uses both the traction boundary element method (TBEM) and the boundary element method (BEM) is proposed to compute the three-dimensional (3D) propagation of elastic waves scattered by two-dimensional (2D) thin rigid inclusions. Although the conventional direct BEM has limitations when dealing with thin-body problems, this model overcomes that difficulty. It is formulated in the frequency domain and, taking into account the 2-1/2D configuration of the problem, can be expressed in terms of waves with varying wavenumbers in the z direction, k_z. The elastic medium is homogeneous and unbounded and it should be noted that no restrictions are imposed on the geometry and orientation of the internal crack.

Keywords: Wave propagation; Elastic scattering; Rigid thin inclusions; Boundary element method; Traction boundary element method; 2-1/2 problem

1. Introduction

The propagation of waves in the vicinity of elastic, empty and rigid thin inclusions and screens has been a topic of interest for many researchers for decades. Solutions have been sought for non-destructive evaluation techniques [1,2], and in seismology (e.g. [3–5]), fracture mechanics [6] and acoustics [7,8].

Different scientific formulations have been developed to study the elastic and acoustic wave scattering by inclusions and thin heterogeneities. Some of the first analytical studies on wave diffraction and scattering focused on the wave motion and reverberations in alluvial basins of regular shape [9,10]. Other work has examined the wave scattering induced by cylindrical circular inclusions and single plane cracks [11–16]. Since these analytical approaches are only known for simple and regular geometries, most researchers have concentrated on developing numerical schemes. The application of purely numerical methods such as the finite elements and the finite differences have mostly been restricted to cases where the response is needed only within localised irregular domains, like soil–structure interaction problems [17–19]. In addition, the boundary element method, the strip element method and a number of hybrid methods have been proposed. The hybrid methods are built by combining several of the other numerical approaches [20–28].

The boundary element method (BEM) is quite suitable, particularly if the solution has to satisfy the far field conditions when the inclusions are buried in an unbounded or half-space elastic medium [29–31]. The BEM requires only the discretization of the surface of the heterogeneities, which is one advantage when compared to some of the other numerical schemes. The classical BEM fails, however, when the body thickness approaches zero, as happens for cracks or thin inclusions.

The modelling of the seismic wave field scattered from an arbitrary number of fractures that are either empty, or contain elastic or fluid material was described by Pointer et al. [5], using an indirect boundary element formulation. The traction boundary integral equation method, a formulation developed from the fields of fracture mechanics and

* Corresponding author. Tel.: +351 239 797201; fax: +351 239 797190.
E-mail address: tadeu@dec.uc.pt (A. Tadeu).

0045-7949/$ - see front matter © 2006 Elsevier Ltd. All rights reserved.
doi:10.1016/j.compstruc.2006.08.034

wave propagation, is capable of dealing with heterogeneities with small thickness [32–35]. Several authors have addressed the problem of evaluating the hypersingular integrals that appear in these formulations (see [36–39]). Prosper [40] and Prosper and Kausel [41] simulated the wave propagation in the vicinity of flat horizontal empty cracks with no thickness in unbounded elastic media, making use of the traction boundary element method (TBEM). They proposed an indirect approach for the analytical evaluation of integrals with hypersingular kernels for the plane-strain cases in the two-dimensional (2D) problem.

In the work described in this paper, the three-dimensional (3D) elastic wave field, scattered by 2D cylindrical thin rigid inclusions or even null-thickness rigid cracks, is evaluated. A frequency domain boundary element formulation is initially outlined, where the displacement boundary integral equation (BEM) is combined with the traction boundary integral equation (TBEM). When the heterogeneity's thickness approaches zero, the combined TBEM + BEM model is employed. When the rigid crack presents no thickness the same formulation is used, with the crack being discretized by coincident lines: the upper part of the crack surface uses one boundary integral equation and the lower part uses the other boundary integral equation. This work follows the developments by Prosper and Kausel [41], but the so called two-and-a-half-dimensional (2-1/2D) problem is now addressed, and the proposed formulations can be applied to rigid cracks of arbitrary shape and orientation, when embedded in unbounded elastic media that can be excited by different kinds of wave sources. Thereafter, comparisons with analytical solutions (for simple geometries and boundary conditions) and two different numerical application cases are presented to demonstrate how efficiently these tools model the elastic wave scattering by rigid cracks.

2. 3D problem formulation

The incident field generated by a harmonic dilatational point source in an unbounded uniform elastic medium with no intrinsic attenuation, can be expressed by means of the classic dilatational potential, ϕ,

$$\phi_{\text{inc}} = \frac{A\mathrm{e}^{\mathrm{i}\frac{\omega}{\alpha}\left(\alpha t-\sqrt{(x-x_s)^2+(y-y_s)^2+(z-z_s)^2}\right)}}{\sqrt{(x-x_s)^2+(y-y_s)^2+(z-z_s)^2}}, \tag{1}$$

in which ω is the oscillating frequency, (x_s, y_s, z_s) is the position of the load, the subscript inc denotes the incident field, A is the wave amplitude, α is the compressional wave velocity of the medium, and $\mathrm{i} = \sqrt{-1}$.

Take an infinite rigid inclusion, with cylindrical geometry, located in such a host elastic medium, and excited by the 3D source given by Eq. (1). Fourier-transforming that equation in the direction in which the geometry of the inclusion remains constant (the z direction), and using the effective wavenumbers, $k_\alpha = \sqrt{\frac{\omega^2}{\alpha^2} - k_z^2}$, with $\mathrm{Im}(k_\alpha) < 0$, where k_z is the axial wavenumber, one obtains:

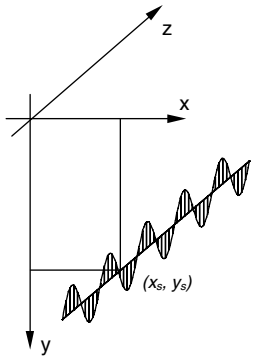

Fig. 1. Harmonic line load varying sinusoidally along the z direction.

$$\hat{\phi}_{\text{inc}}(\omega, x, y, k_z) = \frac{-\mathrm{i}A}{2}\mathrm{H}_0\left(k_\alpha\sqrt{(x-x_s)^2+(y-y_s)^2}\right), \tag{2}$$

in which the $\mathrm{H}_n(\cdots)$ are second kind Hankel functions of the order n.

If an infinite set of evenly-spaced virtual sources along the z direction is assumed, the above incident field may be written as

$$\phi_{\text{inc}}(\omega, x, y, z) = \frac{2\pi}{L_{vs}}\sum_{m=-\infty}^{\infty}\hat{\phi}_{\text{inc}}(\omega, x, y, k_{zm})\mathrm{e}^{-\mathrm{i}k_{zm}z}, \tag{3}$$

where L_{vs} is a spatial source interval large enough to avoid spatial contamination [42], and $k_{zm} = \frac{2\pi}{L_{vs}}m$. Thus, the 3D wave field may be obtained as the wave irradiated by a sum of harmonic (steady-state) line loads whose amplitude varies sinusoidally in the third dimension (see Fig. 1). This sum converges and can be approximated by a finite number of terms [43].

3. Boundary integral formulations

Three different boundary integral formulations are proposed to model wave propagation in elastic media. First, the classical BEM and the TBEM are presented, which allow wave scattering in the neighbourhood of inclusions that are not thin to be simulated. Afterwards, the combination of the BEM and TBEM formulations is presented to model wave propagation through elastic media containing thin rigid inclusions that may even exhibit null-thickness.

3.1. Boundary element formulation (BEM formulation)

Consider a homogeneous elastic medium of infinite extent, which contains a rigid inclusion bounded by a surface S, and is subjected to spatially sinusoidal harmonic line loads placed in the exterior solid medium at $\boldsymbol{x}_s$, with spatial wavenumber k_z. The displacement boundary integral equation can be derived by applying the reciprocity theorem [44], which leads to:

$$0 = \int_S t_j(\boldsymbol{x}, \boldsymbol{n}_n, \omega) G_{ij}(\boldsymbol{x}, \boldsymbol{x}_0, \omega)\, \mathrm{d}s + u_i^{\mathrm{inc}}(\boldsymbol{x}_s, \boldsymbol{x}_0, \omega). \quad (4)$$

In the previous equation, $i,j = 1,2$ represent the normal and tangential directions relative to the inclusion surface, respectively, while $i,j = 3$ correspond to the z direction. $G_{ij}(\boldsymbol{x}, \boldsymbol{x}_0, \omega)$ defines the fundamental solutions for displacements (Green's functions) in the direction j on the boundary S at $\boldsymbol{x}$ caused by a unit point force in the direction i applied at the collocation point, $\boldsymbol{x}_0$. $t_j(\boldsymbol{x}, \boldsymbol{n}_n, \omega)$ specifies the nodal tractions in the direction j on the boundary at $\boldsymbol{x}$. $u_i^{\mathrm{inc}}(\boldsymbol{x}_s, \boldsymbol{x}_0, \omega)$ represents the displacement incident field at $\boldsymbol{x}_0$ along the direction i. The unit outward normal on the boundary at $\boldsymbol{x}$ is defined by the vector $\boldsymbol{n}_n = (\cos\theta_n, \sin\theta_n)$.

The Green's functions for displacements along the x, y and z directions, in the solid medium, are listed in the Appendix, and their derivation can be found at [43].

To evaluate the displacement boundary integral equation, for a general cross-section, both the boundary and boundary values are discretized. A system of linear equations that relates nodal displacements is obtained by successively applying the virtual load to each node on the boundary. Its resolution defines the nodal tractions.

When the element to be integrated is the loaded element, the necessary integrations are performed in closed form [45,46], while numerical integration, performed using a Gaussian quadrature scheme, is used when the element to be integrated is not the loaded one.

3.2. Traction boundary element formulation (TBEM formulation)

However, when modelling rigid inclusions whose thickness approaches zero, the conventional direct boundary element formulation described previously leads to mathematical degenerations. To overcome this difficulty the TBEM can be formulated [40,41] leading to the following traction equation:

$$c_{ij} t_j(\boldsymbol{x}_0, \boldsymbol{n}_n, \omega) = \int_S t_j(\boldsymbol{x}, \boldsymbol{n}_n, \omega) \overline{G}_{ij}(\boldsymbol{x}, \boldsymbol{n}_n, \boldsymbol{x}_0, \omega)\, \mathrm{d}s + \bar{u}_i^{\mathrm{inc}}(\boldsymbol{x}_s, \boldsymbol{x}_0, \boldsymbol{n}_n, \omega). \quad (5)$$

In this equation, $i,j = 1,2$ refer to the normal and tangential directions relative to the inclusion surface, in that order, and $i,j = 3$ stand to the z direction. This traction equation can be interpreted as resulting from the application of dipole loads or dynamic doublets. The coefficient c_{ij} attains $\delta_{ij}/2$, with δ_{ij} the Kronecker delta, when the boundary is smooth. $\overline{G}_{ij}(\boldsymbol{x}, \boldsymbol{n}_n, \boldsymbol{x}_0, \omega)$ are obtained by applying the traction operator to the displacement Green's functions $G_{ij}(\boldsymbol{x}, \boldsymbol{x}_0, \omega)$. This procedure can be taken as the combination of the derivatives of Eq. (4), in order to x, y and z, in such a way as to obtain stresses $\overline{G}_{ij}(\boldsymbol{x}, \boldsymbol{n}_n, \boldsymbol{x}_0, \omega)$. At point $\boldsymbol{x}$ on the boundary element, where the unit outward normal is represented by $\boldsymbol{n}_n = (\cos\theta_n, \sin\theta_n)$, and after performing the equilibrium of stresses, applying loads along the x, y and z directions yields the following equations obtained along x, y and z:

$$\begin{aligned}
\overline{G}_{xr} &= 2\mu\left[\frac{\alpha^2}{2\beta^2}\frac{\partial G_{xr}}{\partial x} + \left(\frac{\alpha^2}{2\beta^2} - 1\right)\left(\frac{\partial G_{yr}}{\partial y} + \frac{\partial G_{zr}}{\partial z}\right)\right]\cos\theta_0 \\
&\quad + \mu\left[\frac{\partial G_{yr}}{\partial x} + \frac{\partial G_{xr}}{\partial y}\right]\sin\theta_0, \\
\overline{G}_{yr} &= 2\mu\left[\left(\frac{\alpha^2}{2\beta^2} - 1\right)\left(\frac{\partial G_{xr}}{\partial x} + \frac{\partial G_{zr}}{\partial z}\right) + \frac{\alpha^2}{2\beta^2}\frac{\partial G_{yr}}{\partial y}\right]\sin\theta_0 \\
&\quad + \mu\left[\frac{\partial G_{yr}}{\partial x} + \frac{\partial G_{xr}}{\partial y}\right]\cos\theta_0, \\
\overline{G}_{zr} &= \mu\left[\frac{\partial G_{xr}}{\partial z} + \frac{\partial G_{zr}}{\partial x}\right]\cos\theta_0 + \mu\left[\frac{\partial G_{yr}}{\partial z} + \frac{\partial G_{zr}}{\partial y}\right]\sin\theta_0,
\end{aligned} \quad (6)$$

with $\boldsymbol{n}_0 = (\cos\theta_0, \sin\theta_0)$ defining the unit outward normal at the collocation point $\boldsymbol{x}_0$, $\overline{G}_{tr} = \overline{G}_{tr}(\boldsymbol{x}, \boldsymbol{n}_n, \boldsymbol{x}_0, \omega)$, $G_{tr} = G_{tr}(\boldsymbol{x}, \boldsymbol{x}_0, \omega)$ and $r,t = x,y,z$.

The incident field components in terms of tractions is given by expressions similar to those for $\overline{G}_{tr}$:

$$\begin{aligned}
\bar{u}_x^{\mathrm{inc}} &= 2\mu\left[\frac{\alpha^2}{2\beta^2}\frac{\partial u_x^{\mathrm{inc}}}{\partial x} + \left(\frac{\alpha^2}{2\beta^2} - 1\right)\left(\frac{\partial u_y^{\mathrm{inc}}}{\partial y} + \frac{\partial u_z^{\mathrm{inc}}}{\partial z}\right)\right]\cos\theta_0 \\
&\quad + \mu\left[\frac{\partial u_y^{\mathrm{inc}}}{\partial x} + \frac{\partial u_x^{\mathrm{inc}}}{\partial y}\right]\sin\theta_0, \\
\bar{u}_y^{\mathrm{inc}} &= 2\mu\left[\left(\frac{\alpha^2}{2\beta^2} - 1\right)\left(\frac{\partial u_x^{\mathrm{inc}}}{\partial x} + \frac{\partial u_z^{\mathrm{inc}}}{\partial z}\right) + \frac{\alpha^2}{2\beta^2}\frac{\partial u_y^{\mathrm{inc}}}{\partial y}\right]\sin\theta_0 \\
&\quad + \mu\left[\frac{\partial u_y^{\mathrm{inc}}}{\partial x} + \frac{\partial u_x^{\mathrm{inc}}}{\partial y}\right]\cos\theta_0, \\
\bar{u}_z^{\mathrm{inc}} &= \mu\left[\frac{\partial u_x^{\mathrm{inc}}}{\partial z} + \frac{\partial u_z^{\mathrm{inc}}}{\partial x}\right]\cos\theta_0 + \mu\left[\frac{\partial u_y^{\mathrm{inc}}}{\partial z} + \frac{\partial u_z^{\mathrm{inc}}}{\partial y}\right]\sin\theta_0
\end{aligned} \quad (7)$$

with $\bar{u}_r^{\mathrm{inc}} = \bar{u}_r^{\mathrm{inc}}(\boldsymbol{x}_s, \boldsymbol{x}_0, \boldsymbol{n}_n, \omega)$, $u_r^{\mathrm{inc}} = u_r^{\mathrm{inc}}(\boldsymbol{x}_s, \boldsymbol{x}_0, \omega)$ and $r = x, y, z$.

These expressions can be combined so as to express $\overline{G}_{ij}(\boldsymbol{x}, \boldsymbol{n}_n, \boldsymbol{x}_0, \omega)$ and $\bar{u}_i^{\mathrm{inc}}(\boldsymbol{x}_s, \boldsymbol{x}_0, \boldsymbol{n}_n, \omega)$ along the normal and tangential directions.

The solutions of the traction boundary integral equation are determined, as in the BEM formulation, by discretizing the boundary into N straight boundary elements, with one nodal point in the middle of each element. This procedure leads to the evaluation of a set of integrals, which are evaluated using a Gaussian quadrature scheme when the element to be integrated is not the loaded element. When the element for which the integration is to be performed is the loaded one, the integration is computed analytically following [45,46].

3.3. TBEM + BEM formulation

The displacement and traction formulations can be combined on opposite collocation points so as to solve the same

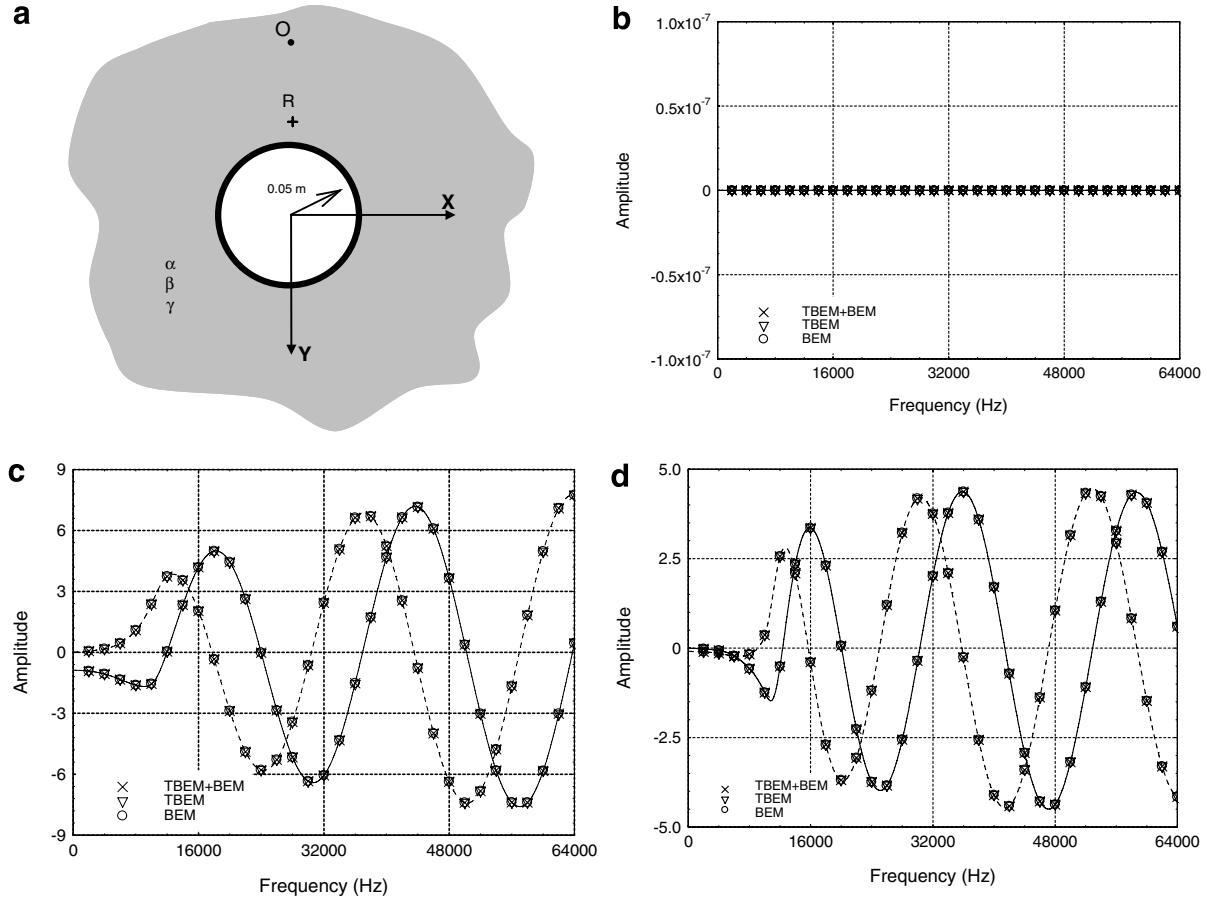

Fig. 2. BEM verification against analytical solution when the medium is excited by a 3D source with $k_z = 25$ rad/m: (a) 2D diagram with problem definition at xy plane; (b) x-displacement component at R; (c) y-displacement component at R; (d) z-displacement component at R.

problems and the cases of thin rigid or even null-thickness inclusions. Part of the boundary surface is loaded with monopole loads (formulation in displacements, using boundary integral equation (4)), while the remaining part is loaded with dipoles (formulation in tractions, using boundary integral equation (5)). In this case, the thin bodies can be solved using a closed surface and the null-thickness rigid heterogeneities are modelled by coincident lines.

4. Verification of the BEM solutions

The wave scattering field generated by a circular rigid cylindrical inclusion, buried in a homogeneous elastic medium, subjected to a point dilatational load can be formulated in a circular cylindrical coordinate system (r, θ, z) and solved by using the separation of variables method [15,47]. This problem was used to corroborate the successful implementation in the frequency domain of the boundary element formulations proposed above. The host elastic medium is unbounded and homogeneous, and is characterized by a mass density $\rho = 2140$ kg/m^3, a dilatational wave speed $\alpha = 2696.5$ m/s and a shear wave speed $\beta = 1451.7$ m/s. The 3D point harmonic load exciting the medium is applied at the source point, O (0.0 m, −0.125 m, 0.0 m), and a receiver is positioned at point R (0.0 m, −0.075 m, 0.0 m), in accordance with Fig. 2a.

Displacements along the x, y and z directions were computed for receiver R in the frequency range from 2000 Hz

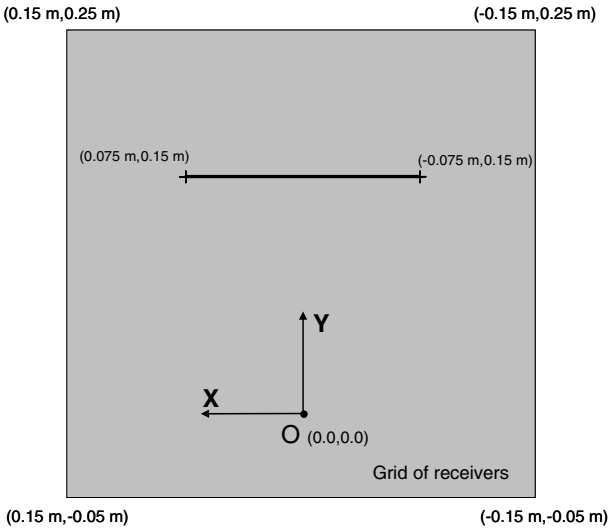

Fig. 3. Geometry of horizontal rigid crack and position of the source (O) and receivers.

to 64,000 Hz, for an axial wavenumber $k_z = 25$ rad/m. The numerical responses in terms of those displacements, obtained by the three boundary element formulations (BEM, TBEM and TBEM + BEM), are plotted against the analytical results in Fig. 2b–d. Both the real and imaginary parts of the responses are shown, and the analytical solution is indicated by solid and dashed lines, respectively, while the marked points refer to the different boundary element models. It can be seen that the agreement between the analytical and numerical results is very good. Also note the agreement between the different boundary element models and that, since the vertical plane corresponding to

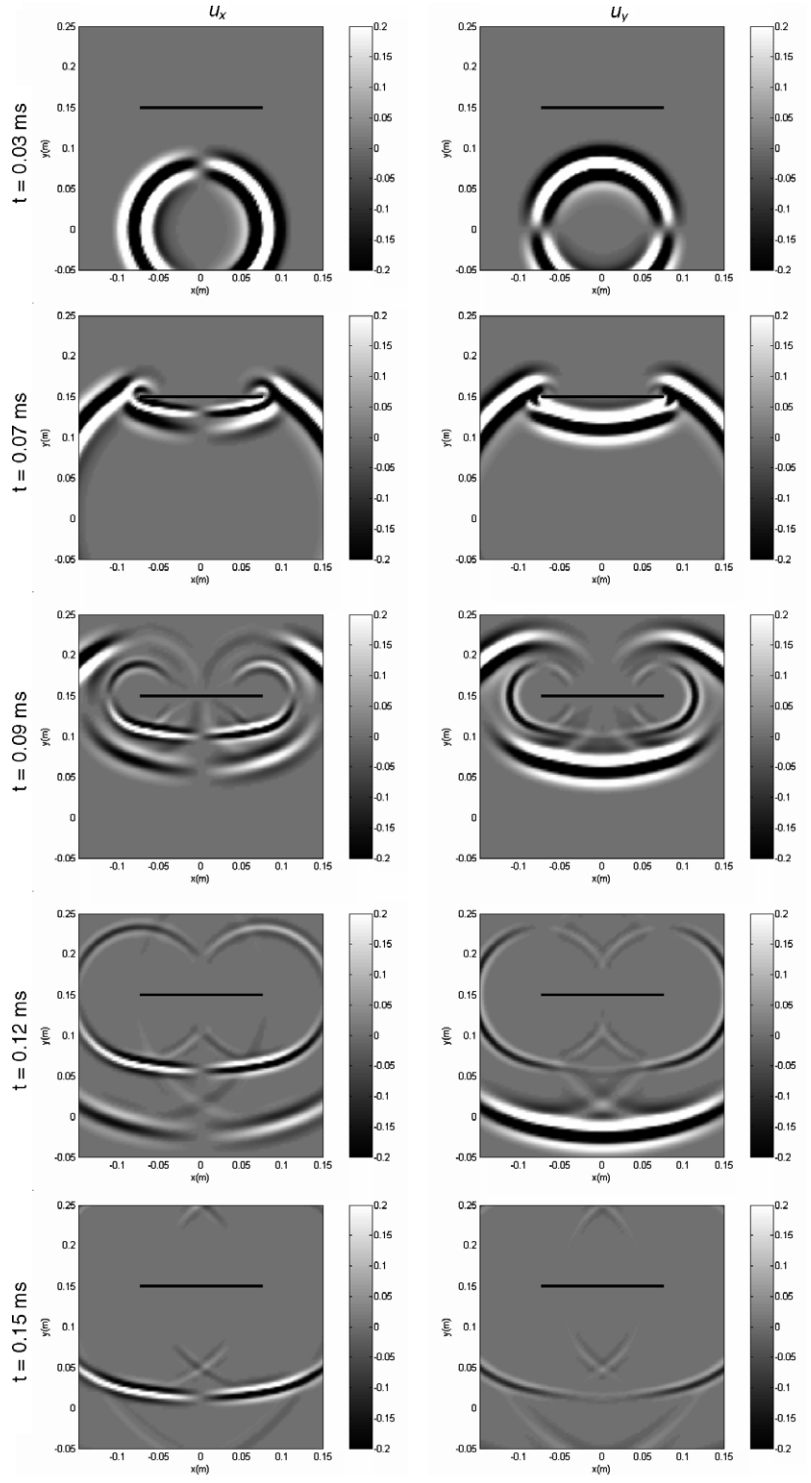

Fig. 4. 2D elastic scattering by a null-thickness horizontal rigid crack in an unbounded medium. x- and y-displacement components (u_x and u_y) at different time instants.

$x = 0.0$ m is a plane of symmetry for loads applied over the y axis, the x-component of displacement at R is null.

5. Responses in time–space

The computations of the boundary element results are performed in the frequency domain for different spatial wavenumbers in the z direction. To obtain time responses for a point harmonic source, the application of discrete Fourier transformations is required in both the wavenumber (k_z) and the frequency (ω) domains. These transformations correspond to the addition of equally spaced virtual contributions at spatial source intervals of $L_{vs} = 2\pi/\Delta k_z$ and time intervals of $T = 2\pi/\Delta\omega$ (with Δk_z and $\Delta\omega$ representing the wavenumber and the frequency increments, respectively).

The time evolution of the dynamic excitation source follows a Ricker pulse, which declines quickly both in time and in frequency. Less computational effort is therefore needed, and it also facilitates the interpretation of the responses in the time–space. The temporal variation of the Ricker function is written as

$$u(\tau) = A(1 - 2\tau^2)\mathrm{e}^{-\tau^2}, \tag{8}$$

where A corresponds to the amplitude; and $\tau = (t - t_s)/t_0$, with t representing the time, t_s the time when the wavelet attains its peak value, and πt_0 the characteristic wavelet period.

After applying a Fourier transformation, this pulse can be expressed in the frequency domain by

$$U(\omega) = A[2t_0\sqrt{\pi}\mathrm{e}^{-\mathrm{i}\omega t_s}]\Omega^2\mathrm{e}^{-\Omega^2} \tag{9}$$

with $\Omega = \omega t_0/2$.

The contamination of the response by the periodic virtual sources (i.e. aliasing phenomena) is avoided by setting intervals between them large enough to guarantee that each contribution arrives later than the time interval T. This is accomplished by introducing complex frequencies with a small imaginary part of the form $\omega_c = \omega - \mathrm{i}\eta$ (with $\eta = 0.7\Delta\omega$), which shifts the frequency axis slightly downwards in the complex plane. This procedure also results in the reduction or elimination of the contribution of the virtual sources. When the time responses are finally evaluated, the effect of using complex frequencies must be taken into account by rescaling the responses with an exponential factor $\mathrm{e}^{\eta t}$ [48].

6. Numerical examples

The combined TBEM + BEM formulation is applied to solve two numerical examples to show its efficiency when dealing with wave propagation in the vicinity of very thin rigid inclusions embedded in elastic unbounded media. First, the evaluation of the 2D wavefield scattered by a horizontal flat rigid crack is presented and analyzed. Then, the 3D wave field generated by a spherical point source in the presence of an S-shaped rigid crack, whose geometry remains constant along the z direction, is computed and discussed.

The boundary element results were obtained by the combined model, with part of the inclusion's surface discretizing the traction boundary integral equation and the opposite part discretizing the displacement boundary integral equation. The selection of the number of boundary elements needed was defined at each calculation frequency by the relation between the wavelength and the length of the boundary elements, and set at 10.

The host elastic medium is the same for both simulations, permitting a dilatational wave velocity of $\alpha = 2696.5$ m/s, and a shear wave velocity of $\beta = 1451.7$ m/s. The results were obtained by performing the computations in the frequency domain, in the frequency range from 2000 Hz to 256,000 Hz, and time signatures were then evaluated by applying an inverse Fourier transformation with the source temporal variation reproducing a Ricker pulse with a characteristic frequency of 75,000 Hz. Since a frequency increment of 2000 Hz is used in the calculations, the limit for the total time window is 0.5 ms.

6.1. 2D example – horizontal flat null-thickness rigid crack

The 2D wave propagation example simulates a horizontal null-thickness rigid crack, embedded in the elastic medium described above. The host medium is excited by a cylindrical source emitting at point O (0.0 m, 0.0 m) as in Fig. 3. The crack is 0.15 m long, located 0.15 m above the source point and the excitation source is centred relative to the y axis. This rigid inclusion is modelled by two coincident horizontal lines with the minimum total boundary elements set to 200, at an initial frequency of 2000 Hz.

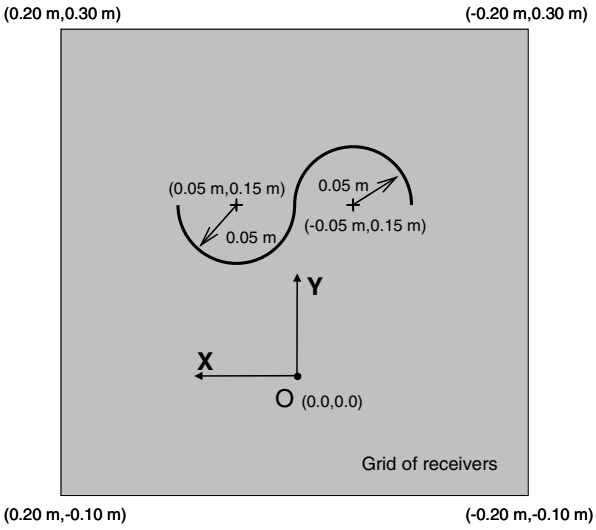

Fig. 5. Geometry of S-shaped rigid crack and position of the source (O) and receivers (2D view at vertical plane $z = 0.0$ m).

Time responses in terms of x- and y-displacement components (u_x and u_y) were computed in a fine grid of receivers evenly spaced along the x and y directions at intervals of 0.003 m and placed around the heterogeneity. The numerical results are presented by time sequential contour plots of the displacement component fields when the waves propagate in the vicinity of the rigid crack (see Figs. 3 and 4). These displacement fields correspond to the incident field generated by the 2D source plus the scattered field by the thin rigid inclusion in the unbounded medium.

In the first two plots, at $t = 0.03$ ms, the waves excited by the dilatational source are propagating in the host medium but they have not yet reached the rigid crack. When the waves hit the thin rigid inclusion, they are totally reflected back as P- and S-waves, but at $t = 0.07$ ms these waves are still undistinguishable as they overlap. At this time instant, the diffracted wave field around the crack is still in its initial development.

The snapshots at $t = 0.09$ ms show very well-developed reflected and diffracted wave fields propagating outwards

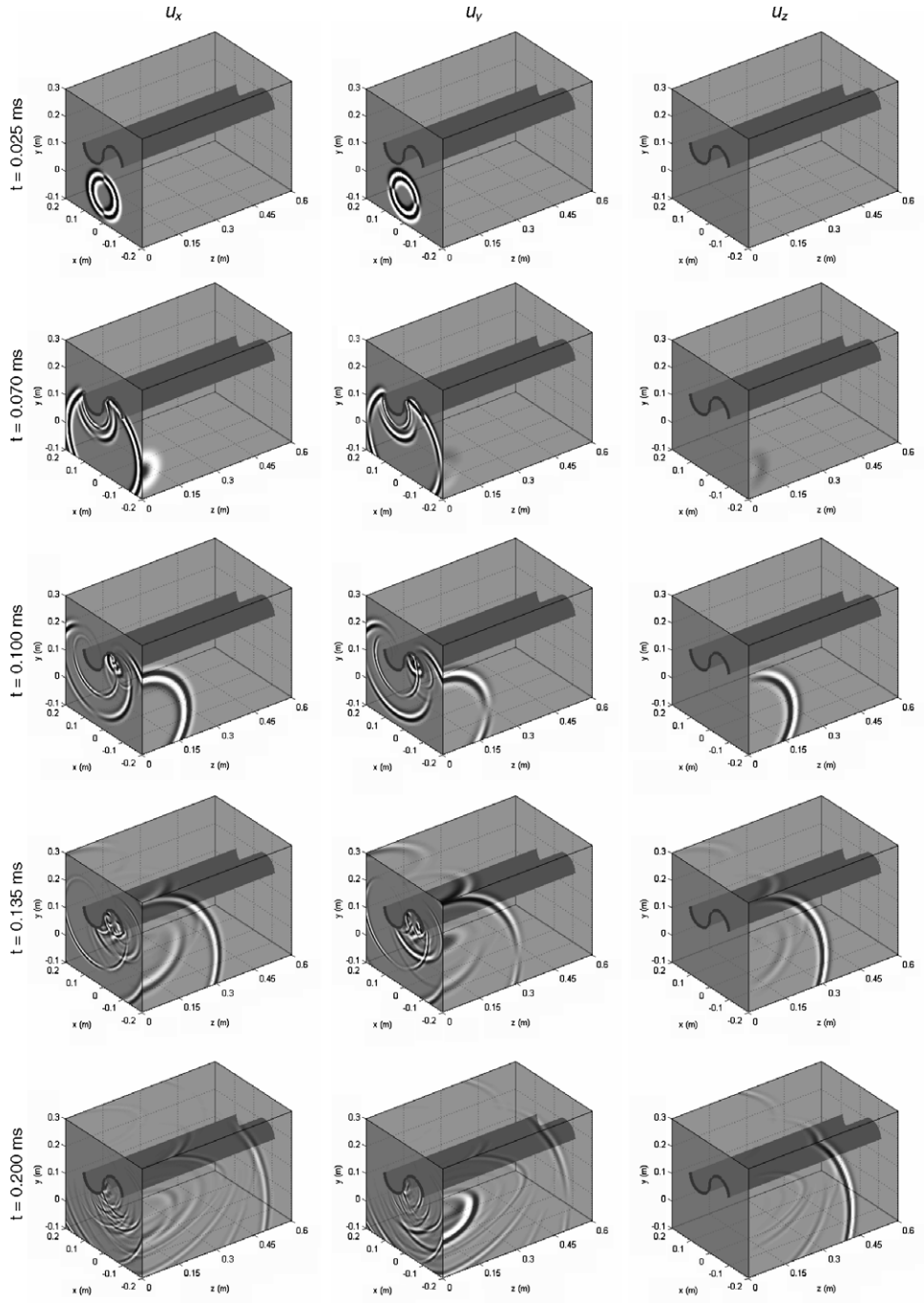

Fig. 6. 3D elastic scattering by a null-thickness S-shaped rigid crack in an unbounded medium. x-, y- and z-displacement components (u_x, u_y and u_z) at different time instants.

from the crack as P- and S-waves. Those waves can be observed propagating at different velocities through the unbounded elastic medium in the last snapshots in Fig. 4.

6.2. 3D example – S-shaped null-thickness rigid crack

The 3D scattered wave field produced by an S-shaped rigid crack, embedded in the unbounded host medium described above, is modelled by means of the combined TBEM + BEM formulation. The elastic medium is excited by a 3D harmonic point load located near the 2-1/2D geometry inclusion. Fig. 5 illustrates the geometry of the S-shaped crack, and the positions of the source point, O (0.0 m, 0.0 m, 0.0 m), and a grid of receivers corresponding to the vertical plane $z = 0.0$ m. The rigid heterogeneity is modelled as a very thin rigid body with zero thickness, discretized by coincident lines with the minimum total boundary elements set to 300, at the first frequency of 2000 Hz.

Numerical responses in the time domain were computed in three fine grids of receivers placed in the host medium along orthogonal planes corresponding to $x = -0.20$ m, $y = 0.30$ m and $z = 0$ m. The receivers are equally spaced at 0.004 m along the x and y directions and at 0.006 m along the longitudinal z direction.

Fig. 6 presents the time evolution of the three displacement component fields (u_x, u_y and u_z) after the source starts exciting the medium at $t = 0.0$ ms. In these plots, the total displacement field is displayed at each receiver, corresponding to the summation of the direct incident field arriving from the point source with the scattered field generated by the rigid inclusion in the unbounded medium. In these 3D snapshots, a gray scale is adopted, where lighter and darker shades are ascribed to higher and lower values of displacement components, respectively.

At the initial time instants, as can be observed at $t = 0.025$ ms in Fig. 6, the propagation of the spherical waves in the elastic medium, diverging away from the source, is still only visible along the vertical plane $z = 0.0$ m. Since the planes $x = 0.0$ m and $y = 0.0$ m correspond to planes of symmetry, the displacement components u_x and u_y are symmetrical before the waves reach the inclusion. Similarly, the displacements u_z are symmetrical in relation to plane $z = 0.0$ m, being null throughout the simulation at the plane of the source. When the elastic waves strike the rigid S-shaped inclusion, at approximately $t = 0.041$ ms on the nearest part of the inclusion to the source point O, the entire wave field is reflected back as P- and S-waves. This is already perceptible at $t = 0.070$ ms, but it is not easy to distinguish the two types of waves since they are almost coincident at this early stage. The wave propagation along the longitudinal direction is also visible from about this time instant onwards along the vertical plane $x = -0.2$ m. At $t = 0.100$ ms, the reflected P- and S-waves are very well developed as they diverge away from the inclusion. The wave energy trapped in the concave part of the inclusion facing the source point generates a complex wave field due to the multiple reflections of the incident waves, which are mostly visible at the vertical plane $z = 0.0$ m. Also note the diffracted wave field getting around the rigid heterogeneity, once the incident pulses reach its extremities. At time $t = 0.135$ ms, the diffracted waves are clearly visible at the horizontal plane $y = 0.3$ m, and a shadow zone has been created, mainly due to the 2-1/2D geometry of the inclusion. Along the plane $x = -0.2$ m the undisturbed incident pulses are followed by the first reflected P-wave pulses for the x-displacement component and reflected P- and S-wave pulses for the y-displacement component. In the last snapshots, the 3D behavior of the scattered wave field by the 2D rigid inclusion is still displayed for all displacement components in the orthogonal grids of receivers.

7. Conclusions

The classical BEM is derived by discretizing the displacement boundary integral equation. When this formulation is applied to problems involving very thin rigid bodies or cracks, it leads to mathematical degenerations and is no longer a valid numerical basis for modelling the wave field scattered by rigid inclusions embedded in unbounded elastic media. In this work, the equation referred to above has been successfully combined with the traction boundary integral equation, and a combined boundary element formulation (TBEM + BEM), that overcomes the thin body difficulty, has been obtained.

The scattering of 3D elastic waves produced by thin rigid inclusions, placed in unbounded 2D media, has therefore been computed numerically using that combined formulation. All integrals with singular kernels are evaluated analytically and no limitation is placed on the geometry and orientation of the heterogeneity, which is discretized with piecewise, straight, constant elements. This model is formulated in the frequency domain and it is expressed as a summation of waves with different spatial wavenumbers in the z direction, since the geometry of these problems is characterised as 2-1/2D. Time signatures are calculated by applying inverse Fourier transforms in both the wavenumber and frequency domains, following the temporal evolution of a Ricker pulse.

The verification of the proposed model was performed by comparing its displacement field, scattered by a circular cylindrical rigid inclusion, with analytical known solutions for this simple geometry and boundary conditions case. For this situation, the results from the displacement boundary integral formulation, from the traction boundary integral formulation and from the combined formulation were in very close agreement with the analytical ones. Two numerical examples, where the elastic wave field scattered by very thin rigid inclusions is numerically evaluated, were used to demonstrate the proposed model's efficiency. The examples were formulated as, first, a horizontal null-thickness rigid inclusion, placed in a two-dimensional unbounded elastic medium that is excited by cylindrical waves, and, second, an S-shaped rigid inclusion, with

constant geometry in the longitudinal direction, embedded in an elastic unbounded medium and excited by a 3D point dilatational source.

Appendix. 2-1/2D Green's functions for unbounded medium

Definitions

$$k_\alpha = \sqrt{\frac{\omega^2}{\alpha^2} - k_z^2}, \quad \text{with } \mathrm{Im}(k_\alpha) < 0,$$

$$k_\beta = \sqrt{\frac{\omega^2}{\beta^2} - k_z^2}, \quad \text{with } \mathrm{Im}(k_\beta) < 0,$$

$$r = \sqrt{(x-x_0)^2 + (y-y_0)^2},$$

$$H_{n\alpha} = \mathrm{H}_n(k_\alpha r), \quad H_{n\beta} = \mathrm{H}_n(k_\beta r), \quad \text{Hankel functions},$$

$$B_n = k_\beta^n H_{n\beta} - k_\alpha^n H_{n\alpha}, \quad B_n \text{ functions}.$$

Green's functions for displacements

$$G_{xx} = \frac{1}{4\mathrm{i}\rho\omega^2}\left[\frac{\omega^2}{\beta^2}H_{0\beta} - \frac{1}{r}B_1 + \left(\frac{x-x_0}{r}\right)^2 B_2\right],$$

$$G_{yy} = \frac{1}{4\mathrm{i}\rho\omega^2}\left[\frac{\omega^2}{\beta^2}H_{0\beta} - \frac{1}{r}B_1 + \left(\frac{y-y_0}{r}\right)^2 B_2\right],$$

$$G_{zz} = \frac{1}{4\mathrm{i}\rho\omega^2}\left[\frac{\omega^2}{\beta^2}H_{0\beta} - k_z^2 B_0\right],$$

$$G_{xy} = G_{yx} = \frac{1}{4\mathrm{i}\rho\omega^2}\left(\frac{x-x_0}{r}\right)\left(\frac{y-y_0}{r}\right)B_2,$$

$$G_{xz} = G_{zx} = \mathrm{i}k_z\frac{1}{4\mathrm{i}\rho\omega^2}\left(\frac{x-x_0}{r}\right)B_1,$$

$$G_{yz} = G_{zy} = \mathrm{i}k_z\frac{1}{4\mathrm{i}\rho\omega^2}\left(\frac{y-y_0}{r}\right)B_1.$$

References

[1] Achenbach JD, Lin W, Keer LM. Mathematical modeling of ultrasonic wave scattering by sub-surface cracks. Ultrasonics 1986; 24:207–15.

[2] Achenbach JD. Modeling for quantitative non-destructive evaluation. Ultrasonics 2002;40:1–10.

[3] Sánchez-Sesma FJ. Diffraction of elastic waves by three dimensional surface irregularities. Bull Seism Soc Am 1983;73:1621–36.

[4] Tadeu AJB, Kausel E, Vrettos C. Scattering of waves by subterranean structures via the boundary element method. Soil Dyn Earthq Eng 1996;15(6):387–97.

[5] Pointer T, Liu E, Hudson JA. Numerical modeling of seismic waves scattered by hydrofractures: application of the indirect boundary element method. Geophys J Int 1998;135:289–303.

[6] Huang JY. Interaction of SH-waves with a finite crack in a half-space. Eng Fract Mech 1995;51(2):217–24.

[7] Lacerda LA, Wrobel LC, Mansur WJ. A dual boundary element formulation for sound propagation around barriers over an infinite plane. J Sound Vib 1997;202:235–347.

[8] Godinho L, António J, Tadeu A. Sound propagation around rigid barriers laterally confined by tall buildings. J Appl Acoust 2002;63(6): 595–609.

[9] Trifunac MD. Surface motion of a semi-cylindrical alluvial valley for incident plane SH waves. Bull Seism Soc Am 1971;61:1755–70.

[10] Wong HL, Trifunac MD. Surface motion of semi-elliptical alluvial valley for incident plane SH-waves. Bull Seism Soc Am 1974;64: 1389–403.

[11] Lee VW. On deformations near circular underground cavity subjected to incident plane SH waves. Symp Appl Comput Methods Eng. Los Angeles: Univ. of Southern California; 1977. p. 951–61.

[12] Datta SK, Shah AH. Scattering of SH-waves by embedded cavities. Wave Motion 1982;4:265–83.

[13] Lee VW. Three-dimensional diffraction of elastic waves by a spherical cavity in an elastic half-space. 1: Closed-form solutions. Soil Dyn Earthq Eng 1988;7:149–61.

[14] Lee VW, Karl JA. Diffraction of SV waves by underground circular cylindrical cavities. Soil Dyn Earthq Eng 1992;11:445–56.

[15] Pao YH, Mow CC. Diffraction of elastic waves and dynamic stress concentrations. Crane and Russak; 1973.

[16] Sánchez-Sesma FJ, Iturrarán-Viveros U. Scattering and diffraction of SH waves by a finite crack: an analytical solution. Geophys J Int 2001;145:749–58.

[17] Waas G. Linear two-dimensional analysis of soil dynamics problems in semi-infinite layered media, PhD Thesis, University of California, Berkeley, CA; 1972.

[18] Lysmer J, Udaka T, Seed HB, Hwang R. LUSH – A computer program for complex response analysis of soil–structure systems. Report No. EERC 74-4, Earthquake Engineering Research Center, University of California, Berkeley, CA; 1974.

[19] Kausel E. Forced vibrations of circular foundations in layered media. MIT Research Report 70-3, Department of Civil Engineering, Massachusetts Institute of Technology, Cambridge, MA; 1974.

[20] Liu GR, Chen SC. Flaw detection in sandwich plates based on time-harmonic response using genetic algorithm. Comput Methods Appl Mech Eng 2001;190:5505–14.

[21] Mahapatra DR, Gopalakrishnan S. Spectral finite element analysis of coupled wave propagation in composite beams with multiple delaminations and strip inclusions. Int J Solids Struct 2004;41:1173–208.

[22] Leutenegger T, Dual J. Detection of defects in cylindrical structures using a time reverse method and a finite-difference approach. Ultrasonics 2002;40:721–5.

[23] Koguchi H, Watabe H. Improving defects search in structure by boundary element and genetic algorithm scan method. Eng Anal Bound Elem 1997;19:105–16.

[24] Richardson JD, Cruse TA. Nonsingular BEM for fracture modelling. Comput Struct 1998;66(5):695–703.

[25] Liu SW, Huang JH, Sung JC, Lee CC. Detection of cracks using neural networks and computational mechanics. Comput Methods Appl Mech Eng 2002;191:2831–45.

[26] Galán JM, Abascal R. Remote characterization of defects in plates with viscoelastic coatings using guided waves. Ultrasonics 2004;42: 877–82.

[27] Weifang Z, Yongdong W, Guorong W, Yide L. Analysis on acoustical scattering by a cracked elastic structure. Acta Mech Solida Sinica 2003;16(3):262–8.

[28] Liu GR. A combined finite element/strip element method for analyzing elastic wave scattering by cracks and inclusions in laminates. Comput Mech 2002;28:76–81.

[29] Stamos AA, Beskos DE. 3-D seismic response analysis of long lined tunnels in half-space. Soil Dyn Earthq Eng 1996;15(2):111–8.

[30] Tadeu A, António J, Kausel E. 3D Scattering of waves by a cylindrical irregular cavity of infinite length in a homogeneous elastic medium. Comput Methods Appl Mech Eng 2002;191(27–28): 3015–33.

[31] Tadeu A, Godinho L. Scattering of acoustic waves by movable lightweight elastic screens. Eng Anal Bound Elem 2003;27(3): 215–26.

[32] Cruse TA. Boundary element analysis in computational fracture mechanics. Kluwer Academic Publishers; 1987.

[33] Sládek V, Sládek J. Transient elastodynamics three-dimensional problems in cracked bodies. Appl Math Model 1984;8:2–10.

[34] Sládek V, Sládek J. A boundary integral equation method for dynamic crack problems. Eng Fract Mech 1987;27(3):269–77.

[35] Takakuda K. Diffraction of plane harmonic waves by cracks. Bull JSME 1983;26(214):487–93.

[36] Rudolphi TJ. The use of simple solutions in the regularisation of hypersingular boundary integral equations. Math Comput Model 1991;15:269–78.
[37] Lutz E, Ingraffea AR, Gray LJ. Use of 'simple solutions' for boundary integral methods in elasticity and fracture analysis. Int J Numer Methods Eng 1992;35:1737–51.
[38] Watson JO. Hermitian cubic boundary elements for plane problems of fracture mechanics. Int J Struct Mech Mater Sci 1982;4:23–42.
[39] Watson JO. Singular boundary elements for the analysis of cracks in plane strain. Int J Numer Methods Eng 1995;38:2389–411.
[40] Prosper D. Modeling and detection of delaminations in laminated plates, PhD Thesis, MIT, Cambridge; 2001.
[41] Prosper D, Kausel E. Wave scattering by cracks in laminated media. In: Atluri SN, Nishioka T, Kikuchi M, editors. CD advances in computational engineering and sciences. Proceedings of the international conference on computational engineering and science, ICES'01. Tech Science Press; 2001.
[42] Bouchon M, Aki K. Discrete wave-number representation of seismic-source wave field. Bull Seism Soc Am 1977;67:259–77.
[43] Tadeu A, Kausel E. Green's functions for two-and-a-half dimensional elastodynamic problems. J Eng Mech 2000;126(10):1093–7.
[44] Manolis GD, Beskos DE. Boundary element methods in elastodynamics. London: Unwin Hyman; 1988. sold to Chapman and Hall.
[45] Tadeu A, Santos P, Kausel E. Closed-form integration of singular terms for constant, linear and quadratic boundary elements – Part I: SH wave propagation. Eng Anal Bound Elem 1999;23(8):671–81.
[46] Tadeu A, Santos P, Kausel E. Closed-form integration of singular terms for constant, linear and quadratic boundary elements – Part II: SV-P wave propagation. Eng Anal Bound Elem 1999;23(9): 757–68.
[47] Tadeu AJB. Modelling and seismic imaging of buried structures, PhD Thesis, MIT, Cambridge; 1992.
[48] Kausel E, Roesset JM. Frequency domain analysis of undamped systems. J Eng Mech 1992;118(4):721–34.